Electric quadrupole moment of the proton halo nucleus ^{8}B

T. Sumikama,[1] T. Nagatomo,[1] M. Ogura,[2] T. Iwakoshi,[2] Y. Nakashima,[2] H. Fujiwara,[2] K. Matsuta,[2] T. Minamisono,[3] M. Fukuda,[2] and M. Mihara[2]

[1]*RIKEN, 2-1 Hirosawa, Wako, Saitama 351-0198, Japan*

[2]*Department of Physics, Osaka University, 1-1 Machikaneyama, Toyonaka, Osaka 560-0043, Japan*

[3]*Fukui University of Technology, 3-6-1 Gakuen, Fukui 910-8505, Japan*

(Received 6 April 2006; published 30 August 2006)

The β-NQR (nuclear quadrupole resonance) signals of ^{8}B ($I^{\pi} = 2^{+}$, $T_{1/2} = 770$ ms) implanted in TiO_2 (rutile) have been detected to determine the electric quadrupole moment of ^{8}B with high precision. The ratio of the quadrupole moments of ^{8}B and ^{12}B was determined as $|Q(^{8}\mathrm{B})/Q(^{12}\mathrm{B})| = 4.88 \pm 0.04$. Combined with the known sign, the quadrupole moment of ^{8}B was obtained as $Q(^{8}\mathrm{B}) = +(64.5 \pm 1.4)$ mb, which is consistent with and more precise than the previously reported value. The experimental values of the Q moment, the proton and neutron radii and the density distribution of ^{8}B were compared with several theoretical predictions and were found to be best reproduced by a microscopic cluster model, which suggests the existence of a proton halo.

DOI: 10.1103/PhysRevC.74.024327 PACS number(s): 21.10.Ky, 27.20.+n

I. INTRODUCTION

The ^{8}B nucleus has a very small proton-separation energy of 137 keV [1], thus it is speculated that the last valence proton of ^{8}B forms a halo structure in spite of the existence of Coulomb and centrifugal barriers. The electric quadrupole (Q) moment reflects not only quadrupole deformation but also spatial spread, especially of the loosely bound proton, because the quadrupole-moment operator includes the square term of distance, i.e., the r^2 term. Guided by this idea, the existence of a proton halo structure has been discussed since the Q moment of ^{8}B was first measured by Minamisono *et al*. in 1992 [2]. The large enhancement of the Q moment from the standard shell-model calculation was connected to the additional spatial spread of the last proton [2], for which the Woods-Saxon potential with the Cohen-Kurath interaction was used. The shell-model calculation using a deformed Woods-Saxon potential [3] showed that a density distribution similar to a proton halo can be postulated, but enhancement of the Q moment cannot be connected mainly to extra enhancement of a proton halo, because the last proton contributes destructively to the Q moment in the case of the ^{8}B nucleus. Several authors calculated the Q moment, as well as the nuclear matter distribution [4–15]. Among the theories that reproduce the Q moment of ^{8}B, some support the proton halo, whereas others do not. At present, the proton, neutron, and matter radii are available, as well as the density distribution of ^{8}B up to 12 fm [16], which were determined by Fukuda *et al*. from the reaction cross sections at several energies from 31 to 790 MeV/nucleon. These authors found that the density distribution has a long tail. Because the Q moment has to be reproduced based on realistic deformation and realistic radial distribution, especially for the loosely bound ^{8}B nucleus, nuclear models should be tested by comparison with all the experimental values for the Q moment, the radii, and the density distribution. In addition, nuclear models should be tested using the mirror partner ^{8}Li, for which the Q moment [17], the radii [18] and the charge radius [19] have been measured.

A systematic uncertainty for the Q-moment value of ^{8}B measured in 1992 may be due to the spread in the β-NQR (nuclear quadrupole resonance) spectrum, owing to both static spread of the electric field gradients in the crystal and the experimental technique, for which the frequency of an rf magnetic field was widely modulated. For correct comparison, confirmation is required using a much improved β-NQR technique, which delivers the opportunity to obtain sharp spectra for both ^{8}B and ^{12}B. A TiO_2 (rutile) crystal is expected to act as a spin Dewar to fully maintain the polarization of various nuclei, such as ^{12}B, ^{12,16}N, ^{13,19}O and ^{41}Sc, at room temperature [20–24]. The hyperfine interactions of ^{12}B ($I^{\pi} = 1^{+}$, $T_{1/2} = 20.20$ ms) implanted in TiO_2 have been studied to determine the electric field gradients in the crystal [20]. Sharp β-NQR spectra obtained for ^{12}B implanted in TiO_2 demonstrated that the ionic crystal was a suitable catcher for boron isotopes. In the present work, we observed the β-NQR spectrum of ^{8}B implanted in TiO_2 to confirm the Q-moment value of ^{8}B with high precision.

II. EXPERIMENTAL PROCEDURE

The experimental setup and procedure are similar to those used in previous studies [2], except for the selection of a TiO_2 implantation catcher and the use of the adiabatic fast passage (AFP) technique for β NQR. A schematic diagram of the experimental setup is shown in Fig. 1.

^{8}B nuclei were produced through the reaction $^{6}\mathrm{Li}(^{3}\mathrm{He}, n)^{8}\mathrm{B}$. A 4.7-MeV ^{3}He beam with a typical intensity of 10 pμA was provided by the Van de Graaff accelerator at Osaka University to bombard an enriched ^{6}LiF target of 317 μg/cm^2, which was evaporated onto a backing made of copper plate using the vacuum evaporation technique. A typical β-ray yield from ^{8}B was 1 kcps. The nuclear-spin polarization of ^{8}B was obtained by selecting the recoil angle of reaction products relative to the incident beam of ^{3}He. The recoil angle was restricted using a recoil collimator to 8°–23° to optimize the

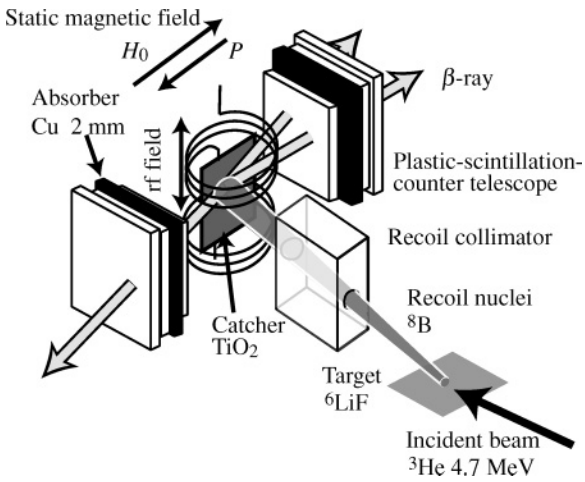

FIG. 1. Schematic diagram of the experimental setup. The recoil angle of ^{8}B was restricted using a recoil collimator to 13° relative to the incident beam of ^{3}He to optimize the nuclear spin polarization produced through the nuclear reaction ^{6}Li(^{3}He, n)^{8}B.

polarization obtained, which was typically 6%. The polarized nuclei were implanted into a TiO_2 catcher (20×20 mm^2 and 300 μm thick) using a recoil energy of approximately 1.9 MeV obtained in the nuclear reaction. The implanted ^{8}B nuclei were distributed from the surface to a maximum depth of approximately 3 μm in the catcher. The c axis was set parallel to the polarization and to the externally applied magnetic field of 300 mT, which was applied to maintain the polarization and for β-NQR detection. The β rays were detected by two sets of plastic scintillation-counter telescopes placed above ($\theta_\beta = 0°$) and below (180°) the catcher, where θ_β is the β-ray ejection angle relative to the polarization axis. Each telescope consisted of three plastic scintillation counters.

Changes in polarization were detected by the change in β-ray angular distribution, which is given by $W(\theta_\beta) \propto (1 + AP\cos\theta_\beta)$, where P is the polarization and $A \approx +1/3$ is the asymmetry parameter. The polarization was inverted using the AFP method during nuclear magnetic resonance (NMR) at the resonance condition. The typical amplitude of the rf oscillating magnetic field was 1.7 mT, the sweep width of the frequency modulation was ±5 kHz and the rf sweep time was 3 ms.

The main contaminants in the catcher, ^{21}Na, ^{20}F, and ^{15}O, were produced by the bombardment of ^{19}F or ^{16}O nuclei contained in the target and in the catcher with the ^{3}He beam. The end-point energies of the main contaminants, however, are smaller than the mean β-ray energy of approximately 7 MeV emitted from ^{8}B [25], with 2.5 MeV for ^{21}Na ($T_{1/2} = 22.5$ s), 5.4 MeV for ^{20}F ($T_{1/2} = 11$ s), and 1.7 MeV for ^{15}O ($T_{1/2} = 122$ s) [26]. To eliminate these low-energy β rays, a copper absorber of 2 mm in thickness was inserted between the first and second counters in each counter set. The fraction of contaminants in the detected β-ray counts was reduced to less than 10^{-3}.

The energy of magnetic substate m of spin I under electric-field gradients (EFGs) superimposed on a high magnetic field H_0 is given by the first-order perturbation theory as:

$$E_m = -\mu H_0 m/I + (3\cos^2\theta - 1 + \eta\sin^2\theta\cos 2\phi) \times\{3m^2 - I(I+1)\}eqQ/8I(2I-1), \quad (1)$$

where θ and ϕ are the Euler angles formed by the directions of H_0 and the EFG. The parameters q and η are given by V_{ii} of the EFGs as $q = V_{zz}$ and $\eta = (V_{xx} - V_{yy})/V_{zz}$, where $|V_{xx}| \leqslant |V_{yy}| \leqslant |V_{zz}|$. V_{ii}, where $i = x$, y, and z, is the second derivative of the electrostatic potential. The frequency ν_m of the transition between neighboring substates $(m-1)$ and m of spin $I = 2$ is given by:

$$\nu_m = \nu_L - \nu_Q(m - 1/2) \times(3\cos^2\theta - 1 + \eta\sin^2\theta\cos 2\phi)/2, \quad (2)$$

where $\nu_L = \mu H_0/Ih$ is the Larmor frequency and $\nu_Q = 3eqQ/2I(2I-1)h$. The β-NQR spectrum, that is, the change in β-ray asymmetry as a function of ν_Q, was detected using multi-rf NMRs [27].

Boron atoms implanted into the TiO_2 (rutile) crystal occupy two implantation sites with relative populations 9 : 1, of which the major site is suggested to be a Ti substitutional site and the minor one to be an octahedral interstitial site [20,28]. We manipulated the nuclear spin of ^{8}B implanted in the major site, for which the direction of q was parallel to the c axis and $\eta < 0.03$. In the present experiment, the c axis was set parallel to the static magnetic field, i.e., $\theta = 0°$.

The timing program shown in Fig. 2 was used to observe the β-NQR spectrum. Polarized ^{8}B was produced during a beam bombardment time of 800 ms. The polarization was fully inverted at the resonance condition by applying a series of 10 rfs at four different frequencies. There were two β-ray count sections after each beam pulse. The counting time was 300 ms for the first section and 600 ms for the last section. The direction of the polarization at the resonance condition is shown in Fig. 2. From four up/down counting rate ratios (U/D) in the two beam-count cycles, the asymmetry change $\Delta(\mathrm{AFP}) = [(\mathrm{U/D})_\mathrm{I}(\mathrm{U/D})_\mathrm{IV}(\mathrm{U/D})_\mathrm{II}^{-1}(\mathrm{U/D})_\mathrm{III}^{-1} - 1] \simeq 8A\Delta P$ was obtained, where ΔP is the fraction of polarization inverted by multi-rf NMRs.

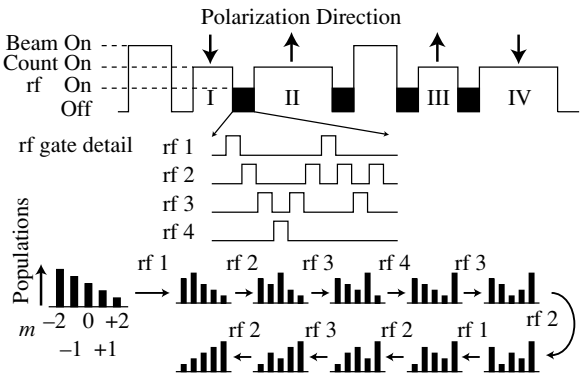

FIG. 2. Timing program for the pulsed beam and the gates for count and rf and spin manipulation. The AFP methods labeled rf 1, 2, 3, and 4 exchange two populations between neighboring magnetic substates $m = -2$ and -1, $m = -1$ and 0, $m = 0$ and $+1$, and $m = +1$ and $+2$, respectively.

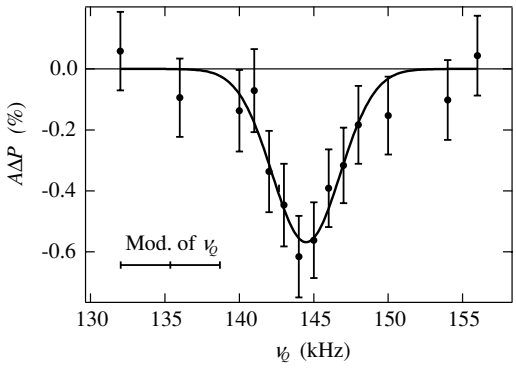

FIG. 3. β-NQR spectrum of ^{8}B in TiO_2. The horizontal bar shows the ν_Q region swept by frequency modulation (FM) of ±5 kHz, corresponding to ±3.3 kHz for ν_Q. The vertical axis is the product of the asymmetry parameter and the polarization change. The solid line shows the best-fit Gaussian distribution.

III. RESULTS AND DISCUSSION

The β-NQR spectrum of ^{8}B implanted in the major site of TiO_2 was obtained as a function of $\nu_Q = eqQ/4h$, as shown in Fig. 3. The spread of the spectrum resulted mainly from the static spread of the EFG. From χ^2-fitting analysis using the Gaussian distribution, the quadrupole coupling frequency $\nu_Q(^8\mathrm{B}) = (144.5 \pm 0.4 \pm 0.4)$ kHz was obtained, where the second error denotes the systematic uncertainty that may be caused by the static spread of the EFG and by an ambiguity in the frequency-swept region of an rf magnetic field. Combined with $\nu_Q(^{12}\mathrm{B}) = (177.7 \pm 0.6 \pm 1.5)$ kHz for ^{12}B in the same site [20], the ratio of Q moments of ^{8}B and ^{12}B was determined as $|Q(^8\mathrm{B})/Q(^{12}\mathrm{B})| = 4.88 \pm 0.02 \pm 0.04$. The results were compared with previous values, which were obtained using a Mg catcher, as shown in Table I. Two experiments were performed using different rods of a single crystal of Mg and different techniques were applied to an rf magnetic field. The static spread of ν_Q observed previously [2] was due to the poor quality of the single crystal and may have led to underestimated uncertainty of 1.5 kHz for ν_Q. The wider frequency modulation applied by Ohi *et al.* [29] than in the present experiment led to larger systematic uncertainty. The present ratio of the Q moments determined with the TiO_2 catcher is more precise and consistent with that for the Mg catcher used by Ohi *et al.* [29]. Combined with the Q moment of ^{12}B, $|Q(^{12}\mathrm{B})| = (13.21 \pm 0.26)$ mb [2], and the sign $Q(^8\mathrm{B}) > 0$ [30], the Q moment of ^{8}B was determined precisely as $Q(^8\mathrm{B}) = +(64.5 \pm 1.4)$ mb.

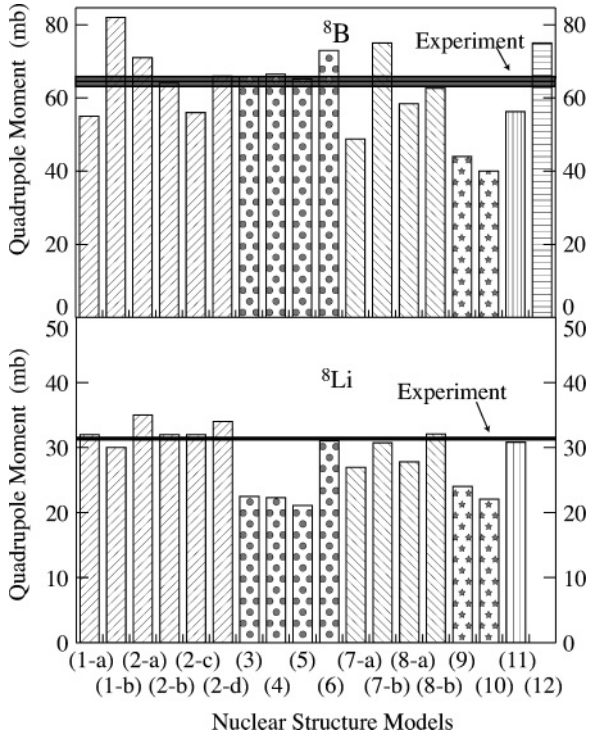

FIG. 4. Experimental and theoretical Q moments of mirror nuclei ^{8}B and ^{8}Li. Numbers in parentheses denote the nuclear models as summarized in Table II.

The present Q moment of ^{8}B was compared with the theoretical calculations [4–15] in Fig. 4, together with that of the mirror partner ^{8}Li, $Q(^8\mathrm{Li}) = +(31.4 \pm 0.2)$ mb [17]. The references of nuclear models denoted by numbers in parentheses are summarized in Table II. The bars for models (1) and (2) in Fig. 4 are predictions by *ab initio* calculations [4,5]; model (1-a) is the variational Monte Carlo (VMC) method, model (2-a) is the Green's function Monte Carlo method (GFMC) with the two-body interaction Argonne $v8$ (AV8), and models (1-b), (2-b), (2-c), and (2-d) are the GFMC with the two-body interaction AV18 and the three-body interactions Urbana IX, Illinois (IL) 2, IL3, and IL4, respectively. The bars for models (3), (4), (5), and (6) are by the microscopic cluster models [6–9]. The bars for models (7) and (8) are by shell model calculations [10,11] with the empirical effective interaction. Models (7-a) and (7-b) are based on the harmonic-oscillator wave function and the Woods-Saxon wave function with the Cohen-Kurath interaction [31], respectively. Models (8-a) and (8-b) are based on the harmonic-oscillator wave functions

TABLE I. Quadrupole coupling frequency ν_Q, static spread $\delta\nu_Q$ (half width at half maximum) of ν_Q, frequency modulation of ν_Q, technique applied to the rf magnetic field and the ratio of $Q(^8\mathrm{B})$ to $Q(^{12}\mathrm{B})$ for Mg and TiO_2 catchers. Second errors of ν_Q and $|Q(^8\mathrm{B})/Q(^{12}\mathrm{B})|$ denote a systematic uncertainty.

Catcher	ν_Q (kHz)	$\delta\nu_Q$ (kHz)	Mod. of ν_Q (kHz)	Technique	$\lvert Q(^8\mathrm{B})/Q(^{12}\mathrm{B})\rvert$	Reference
TiO_2	$144.5 \pm 0.4 \pm 0.4$	2.5	±3.3	AFP	$4.88 \pm 0.02 \pm 0.04$	Present
Mg	$57.5 \pm 0.2 \pm 1.0$	<4	±10	AFP	$4.89 \pm 0.02 \pm 0.09$	[29]
Mg	$60.9 \pm 1.5 \pm 1.5$	15	±10	Depolarization	$5.18 \pm 0.13 \pm 0.13$	[2]

TABLE II. References of the nuclear structure models discussed in this article.

Model	Comment	Author(s)	Reference
(1)	VMC and GFMC with AV18+Urbana IX	Wiringa *et al.*	[4]
(2)	GFMC with AV8 or AV18+IL2, IL3, or IL4	Pieper *et al.*	[5]
(3)	Microscopic cluster model	Csótó *et al.*	[6]
(4)	Microscopic cluster model	Varga *et al.*	[7]
(5)	Microscopic cluster model	Grigorenko *et al.*	[8]
(6)	Microscopic cluster model	Baye *et al.*	[9]
(7)	Shell-model with Cohen-Kurath interaction	Kitagawa *et al.*	[10]
(8)	Shell-model with Walters interaction	Nakada *et al.*	[11]
(9)	Shell-model based on two-body interaction	Coraggio *et al.*	[12]
(10)	Shell-model based on two-body interaction	Navrátil *et al.*	[13]
(11)	Hartree Fock	Kitagawa	[14]
(12)	Relativistic mean field	Patra *et al.*	[15]

with the Wolters interaction [32] and with no effective charge and with small effective charges, respectively. The bars for models (9) and (10) are by shell-model calculations [12,13] with effective interaction based on the two-body interaction, model (11) is by the Hartree Fock method [14] and model (12) is by the relativistic mean field [15].

The *ab initio* calculations, models (1) and (2), reproduce fairly well the Q moments of the mirror nuclei. The contribution of the three-body interaction is clearly observed in the Q moment of ^{8}B, and the realistic three-body interactions of IL2 and IL4 seem to be quite suitable. Although the *ab initio* calculation with the two-body interaction (2-a) reproduces the Q moments of the mirror nuclei fairly well, shell-model calculations with the two-body interaction, models (9) and (10), are too small. This may suggest that it is difficult to reproduce quadrupole deformation using harmonic-oscillator (HO) wave functions, even with a large $4\hbar\omega$ model space. Even if HO wave functions are used, the Q moments are well reproduced by the shell-model calculation (8-b) with the proper empirical effective interaction. We cannot check whether this calculation describes well the long tail distribution of ^{8}B, in spite of the HO potential or not, because the radius was not reported by Nakada and Otsuka [11]. Although the microscopic cluster model reproduces well the Q moment of ^{8}B, it fails to reproduce the Q moment of ^{8}Li. Because the neutron separation energy of 2 MeV is large, the cluster picture consisting of n, t, and α particles may differ from the realistic structure of ^{8}Li.

To investigate which models describe well the ^{8}B ground-state properties of the spatial deformation and the density distribution, we compared the theoretical calculations with the experimental values for the Q moments and the proton or neutron radius. Figures 5 and 6 show the ratio for calculated

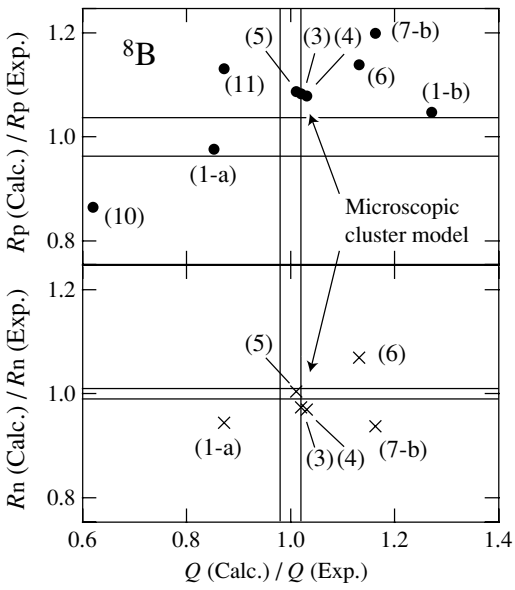

FIG. 5. Ratio of the calculated to experimental values for the Q moment and the proton or neutron radius of ^{8}B. Numbers in parentheses are as for Fig. 4. The upper and the lower figures show the Q moments versus the proton and neutron radius, respectively. The bands show the experimental errors.

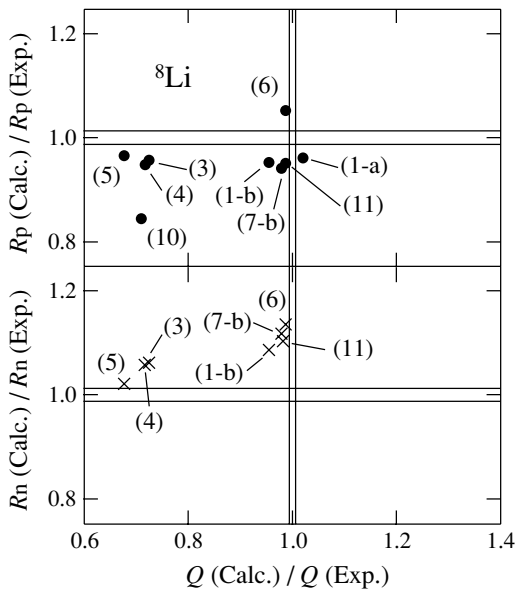

FIG. 6. Ratio of the calculated to experimental values for the Q moment and the proton or neutron radius of ^{8}Li.

to experimental values for ^{8}B and ^{8}Li, respectively. Here, we show only the models that calculate both the Q moment and the proton or neutron radius. It seems to be more difficult to reproduce the Q moment than the proton and neutron radii, especially for ^{8}B. This indicates that the Q moment is a good probe for understanding the behavior of the loosely bound system. Although many models simultaneously reproduce both the Q moment and the radii for ^{8}Li within $\pm 10\%$ accuracy, only the microscopic cluster model of (3), (4), and (5) reproduces both values for ^{8}B, but fails badly for ^{8}Li. Furthermore, model (4) reproduces quite well the density distribution of ^{8}B extracted from the reaction cross sections [7,16]. The density distribution of model (5) is expected to be the same as that of (4) referred to by Fukuda *et al.* [16], because the predictions of the Q moment and the nuclear radii are consistent with each other. Our measurement, therefore, supports the halo structure predicted by the microscopic cluster model of (5), for which a long tail for ^{8}B is clearly observed in the spatial correlation density between p and ^{7}Be, and the valence proton radius is greater than the radius of the ^{7}Be core by 75%.

IV. CONCLUSION

The β-NQR spectrum of ^{8}B implanted in single-crystal TiO_2 (rutile) was observed. The ratio of the electric Q moment of ^{8}B and ^{12}B, and the Q moment of ^{8}B were determined. The Q moment and the proton and neutron radii were compared with various models. Good agreement within 10% was found for the microscopic cluster model, which predicts a long tail in the density distribution, corresponding most likely to a proton halo.

ACKNOWLEDGMENTS

This work was supported in part by Grants-in-Aid for Scientific Research. T. S. acknowledges the Special Postdoctoral Researcher Program of RIKEN for financial support.

[1] G. Audi, O. Bersillon, J. Blachot, and A. H. Wapstra, Nucl. Phys. **A729**, 3 (2003).
[2] T. Minamisono, T. Ohtsubo, I. Minami, S. Fukuda, A. Kitagawa, M. Fukuda, K. Matsuta, Y. Nojiri, S. Takeda, H. Sagawa, and H. Kitagawa, Phys. Rev. Lett. **69**, 2058 (1992).
[3] A. Muta and T. Otsuka, Prog. Theor. Phys. Suppl. **142**, 355 (2001).
[4] R. B. Wiringa, S. C. Pieper, J. Carlson, and V. R. Pandharipande, Phys. Rev. C **62**, 014001 (2000).
[5] S. C. Pieper, V. R. Pandharipande, R. B. Wiringa, and J. Carlson, Phys. Rev. C **64**, 014001 (2001).
[6] A. Csótó, Phys. Lett. **B315**, 24 (1993).
[7] K. Varga, Y. Suzuki, and I. Tanihata, Phys. Rev. C **52**, 3013 (1995).
[8] L. V. Grigorenko, B. V. Danilin, V. D. Efros, N. B. Shul'gina, and M. V. Zhukov, Phys. Rev. C **57**, 2099(R) (1998).
[9] D. Baye, P. Descouvemont, and N. K. Timofeyuk, Nucl. Phys. **A577**, 624 (1994); **A588**, 147c (1995).
[10] H. Kitagawa and H. Sagawa, Phys. Lett. **B299**, 1 (1993).
[11] H. Nakada and T. Otsuka, Phys. Rev. C **49**, 886 (1994).
[12] L. Coraggio, A. Covello, A. Gargano, N. Itaco, and T. T. S. Kuo, J. Phys. G: Nucl. Part. Phys. **27**, 2351 (2001).
[13] P. Navrátil and B. R. Barrett, Phys. Rev. C **57**, 3119 (1998).
[14] H. Kitagawa, Prog. Theor. Phys. **102**, 1015 (1999).
[15] S. K. Patra, C.-L. Wu, and C. R. Praharaj, Mod. Phys. Lett. A **13**, 2743 (1998).
[16] M. Fukuda, M. Mihara, T. Fukao, S. Fukuda, M. Ishihara, S. Ito, T. Kobayashi, K. Matsuta, T. Minamisono, S. Momota *et al.*, Nucl. Phys. **A656**, 209 (1999).
[17] D. Borremans, D. L. Balabanski, K. Blaum, W. Geithner, S. Gheysen, P. Himpe, M. Kowalska, J. Lassen, P. Lievens, S. Mallion *et al.*, Phys. Rev. C **72**, 044309 (2005).
[18] I. Tanihata, T. Kobayashi, O. Yamakawa, S. Shimoura, K. Ekuni, K. Sugimoto, N. Takahashi, T. Shimoda, and H. Sato, Phys. Lett. **B206**, 592 (1988).
[19] R. Sánchez, W. Nörtershäuser, G. Ewald, D. Albers, J. Behr, P. Bricault, B. A. Bushaw, A. Dax, J. Dilling, M. Dombsky *et al.*, Phys. Rev. Lett. **96**, 033002 (2006).
[20] M. Ogura, K. Minamisono, T. Sumikama, T. Nagatomo, T. Iwakoshi, T. Miyake, K. Hashimoto, S. Kudo, K. Arimura, M. Ota *et al.*, Hyperfine Interact. **136/137**, 195 (2001).
[21] T. Minamisono, K. Sato, H. Akai, S. Takeda, Y. Maruyama, K. Matsuta, M. Fukuda, T. Miyake, A. Morishita, T. Izumikawa *et al.*, Z. Naturforsch. **53A**, 293 (1998).
[22] T. Minamisono, Y. Nojiri, K. Matsuta, M. Fukuda, K. Sato, M. Tanigaki, A. Morishita, T. Miyake, Y. Matsumoto, T. Onishi *et al.*, Phys. Lett. **B457**, 9 (1999).
[23] K. Matsuta, K. Sato, M. Fukuda, M. Mihara, T. Yamaguchi, M. Sasaki, T. Miyake, K. Minamisono, T. Minamisono, M. Tanigaki *et al.*, Phys. Lett. **B459**, 81 (1999).
[24] T. Minamisono, S. Fukuda, T. Ohtsubo, A. Kitagawa, Y. Nakayama, Y. Someda, S. Takeda, M. Fukuda, K. Matsuta, and Y. Nojiri, Nucl. Phys. **A559**, 239 (1993).
[25] D. R. Tilley, J. H. Kelley, J. L. Godwin, D. J. Millener, J. E. Purcell, C. G. Sheu, and H. R. Weller, Nucl. Phys. **A745**, 155 (2004).
[26] R. B. Firestone, Nucl. Data Sheets **103**, 269 (2004); D. R. Tilley, C. M. Cheves, J. H. Kelley, S. Raman, and H. R. Weller, Nucl. Phys. **A636**, 249 (1998); F. Ajzenberg-Selove, *ibid.* **A523**, 1 (1991).
[27] T. Minamisono, T. Ohtsubo, S. Fukuda, I. Minami, Y. Nakayama, M. Fukuda, K. Matsuta, and Y. Nojiri, Hyperfine Interact. **80**, 1315 (1993).
[28] T. Sumikama, M. Ogura, Y. Nakashima, T. Iwakoshi, M. Mihara, M. Fukuda, K. Matsuta, T. Minamisono, and H. Akai, Hyperfine Interact. **158**, 413 (2004).
[29] S. Ohi, F. Ohsumi, Y. Muramoto, Y. Naruse, T. Yamaguchi, T. Miyake, K. Matsuta, M. Fukuda, Y. Nojiri, and T. Minamisono, in *OULNS Annual Report* (1995), p. 71.
[30] T. Yamaguchi, K. Sato, C. Ha, A. Morishita, K. Tanaka, T. Miyake, M. Sasaki, K. Minamisono, H. Akai, M. Mihara *et al.*, Hyperfine Interact. **120/121**, 689 (1999).
[31] S. Cohen and D. Kurath, Nucl. Phys. **73**, 1 (1965).
[32] A. A. Wolters, A. G. M. van Hees, and P. W. M. Glaudemans, Phys. Rev. C **42**, 2053 (1990); **42**, 2062 (1990).